ADVANCED ENERGY MATERIALS

Supporting Information

for *Adv. Energy Mater.,* DOI: 10.1002/aenm.202203969

Unveiling the Mechanical and Electrochemical Evolution of Nanosilicon Composite Anodes in Sulfide-Based All-Solid-State Batteries

Daxian Cao, Tongtai Ji, Avtar Singh, Seongmin Bak, Yonghua Du, Xianghui Xiao, Hongyi Xu, Juner Zhu,* and Hongli Zhu**

Supporting Information

Unveiling the Mechanical and Electrochemical Evolution of Nano Silicon Composite Anodes in Sulfide based All-solid-state Batteries

Daxian Cao[1,#], Tongtai Ji[1,#], Avtar Sing[2,#], Seongmin Bak[3], Yonghua Du[3], Xianghui Xiao[3], Hongyi Xu[4,], Juner Zhu[1,*], Hongli Zhu[1,*]*

[1]Department of Mechanical and Industrial Engineering, Northeastern University, Boston, Massachusetts 02115, USA.

[2]Center for Energy Conversion and Storage Systems, National Renewable Energy Laboratory, Golden, CO 80401, USA

[3]National Synchrotron Light Source II, Brookhaven National Laboratory, Upton, NY 11973, USA

[4]Department of Mechanical Engineering, University of Connecticut, Storrs, CT 06269, USA

*: Corresponding author: Hongli Zhu (h.zhu@northeastern.edu);

Juner Zhu (j.zhu@northeastern.edu);

Hongyi Xu (hongyi.3.xu@uconn.edu)

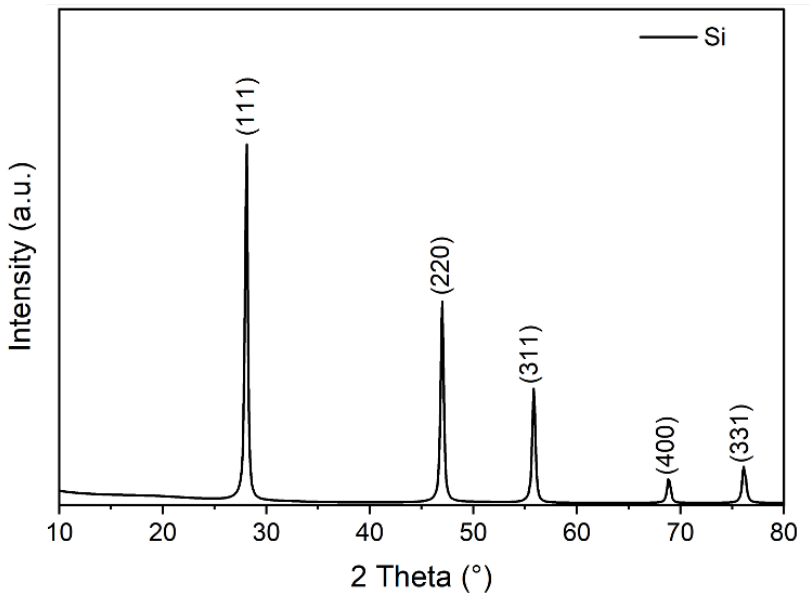

Figure S1. XRD of nano Si

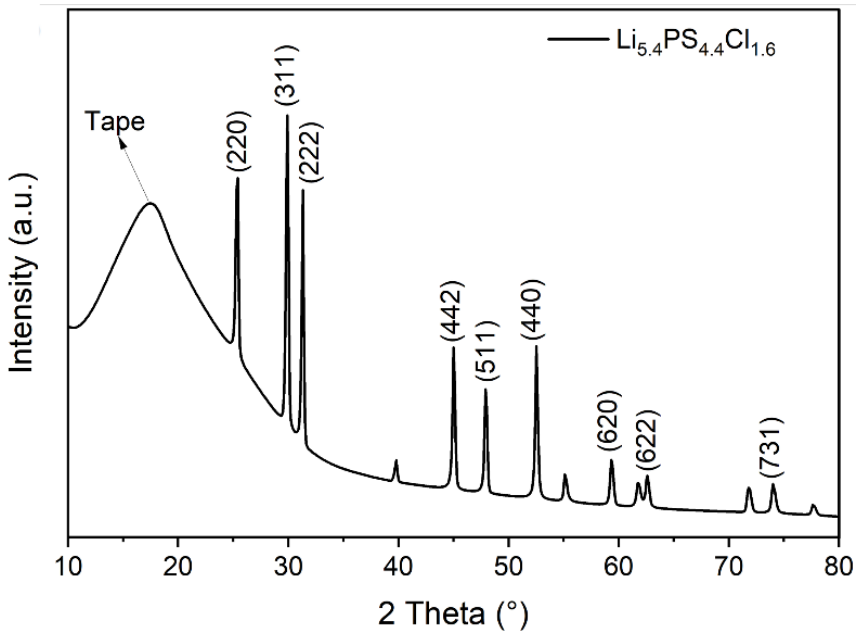

Figure S2. XRD of $Li_{5.4}PS_{4.4}Cl_{1.6}$

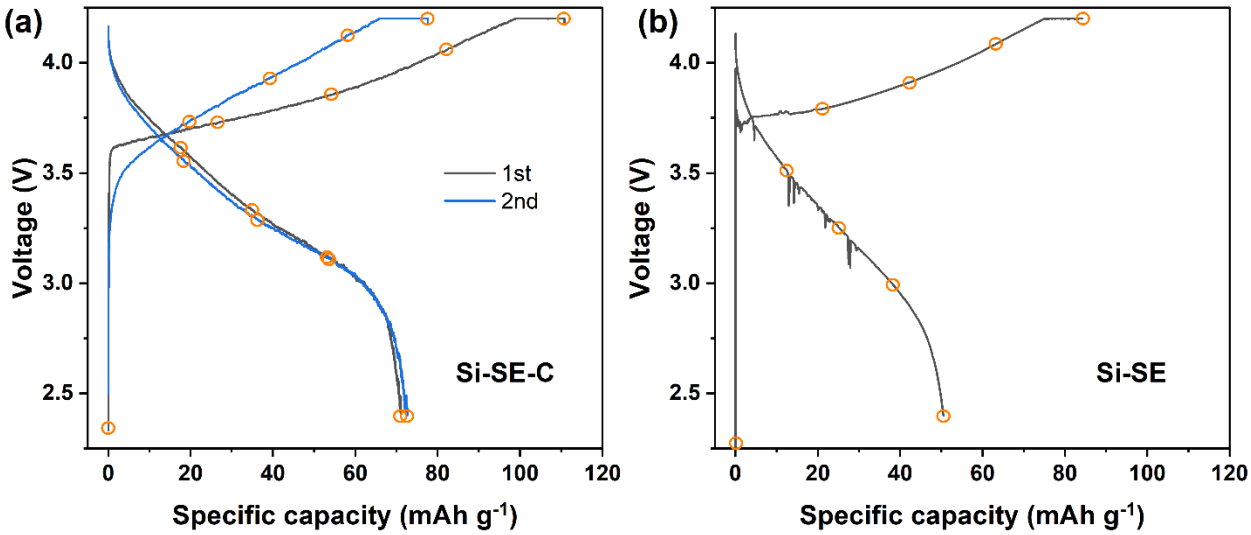

Figure S3 Charge and discharge profiles in full cells using (a) Si-SE-C and (b) Si-SE as anodes during the operando XANES test. The orange circle marked the position of different SoC and DoD.

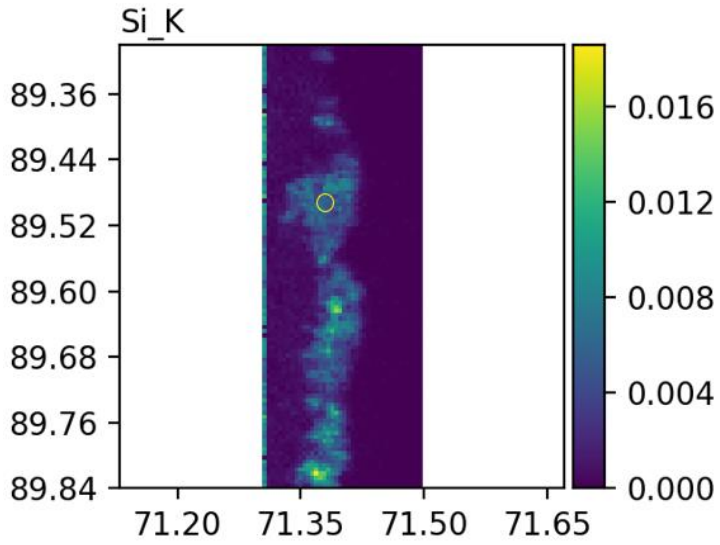

Figure S4. Si K-edge X-ray fluorescence mapping to show the distribution of Si at the cross section in Si-SE-C. The *operando* Sulfur K-edge XANES spectra were collected at the position marked with circle.

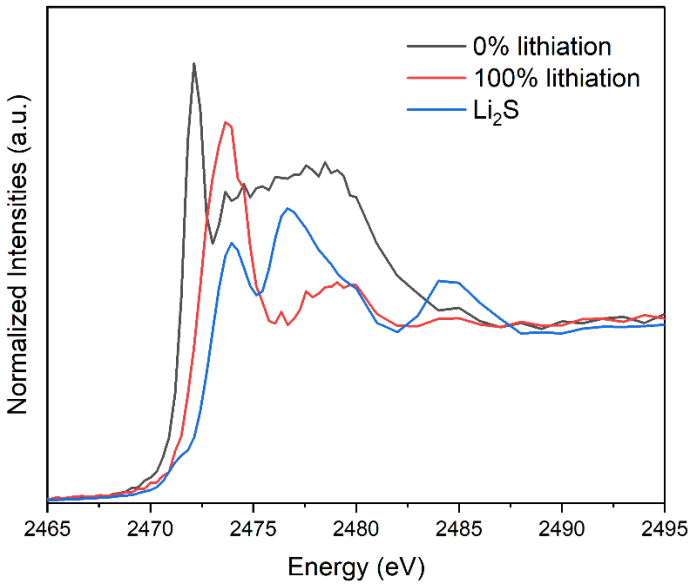

Figure S5. Sulfur K-edge XANES spectra of Si composite anode at 0% lithiation and 100% lithiation states in comparison to the Li_2S.

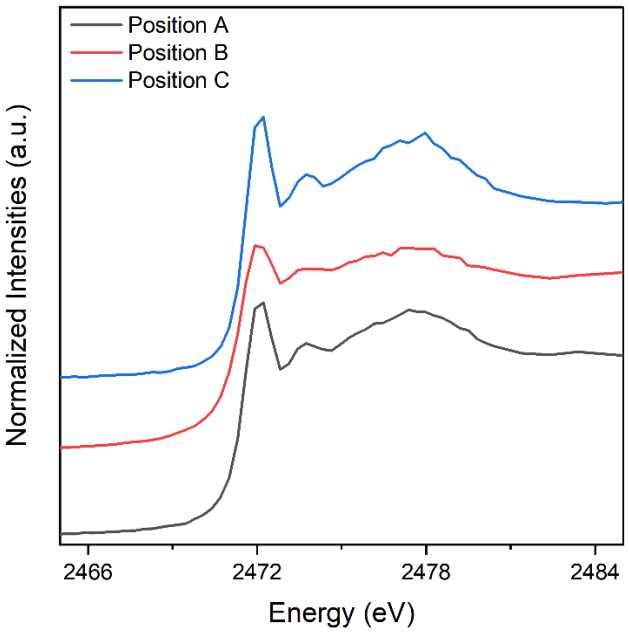

Figure S6. Sulfur K-edge XANES spectra of Si composite anode at 100% lithiation states in other positions.

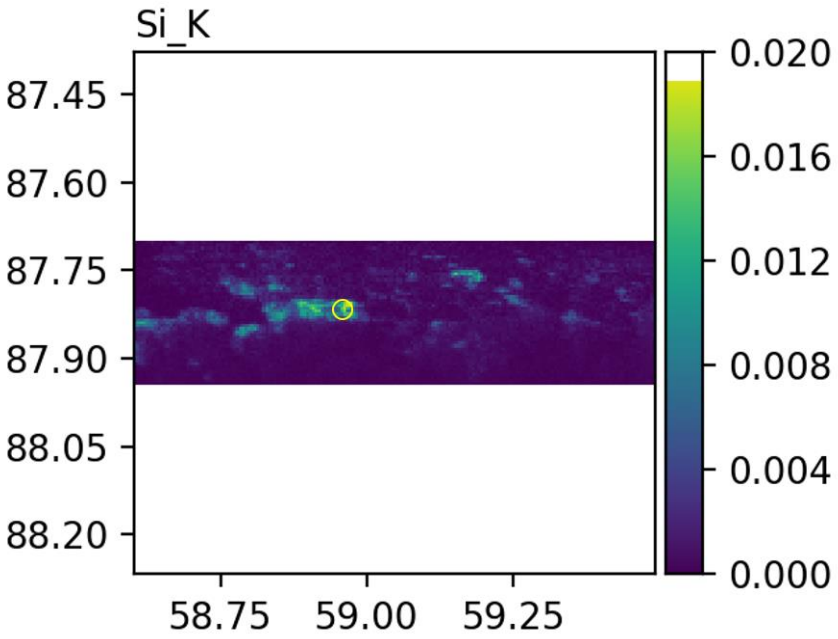

Figure S7. Si K-edge X-ray fluorescence mapping to show the distribution of Si at the cross section in Si-SE. The *operando* Sulfur K-edge XANES spectra were collected at the position marked with circle.

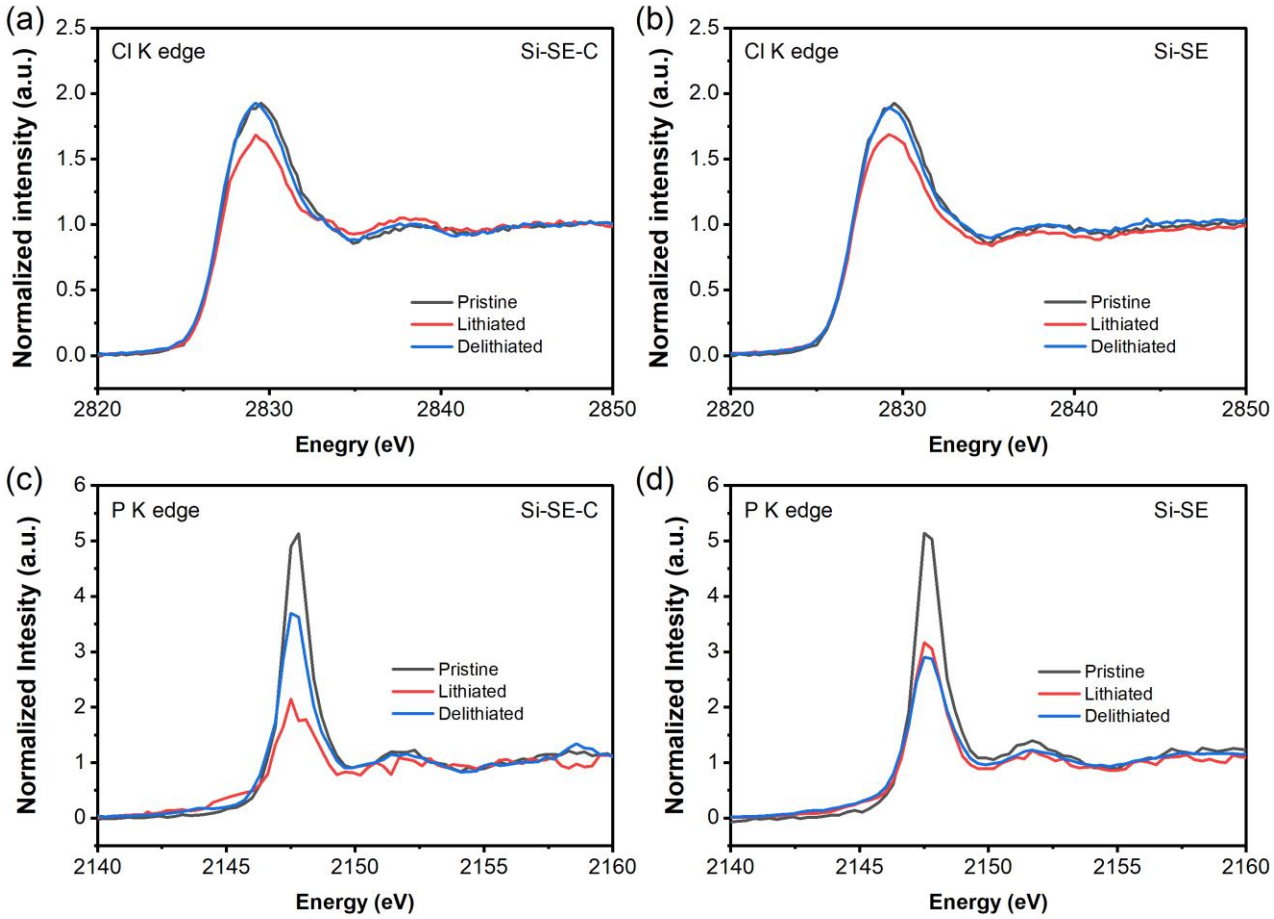

Figure S8. Cl K edge XANES spectra comparison of (a) Si-SE-C and (b) Si-SE composite anode at pristine, lithiated, and delithiated states. P K edge XANES spectra comparison of (a) Si-SE-C and (b) Si-SE composite anode at pristine, lithiated, and delithiated states.

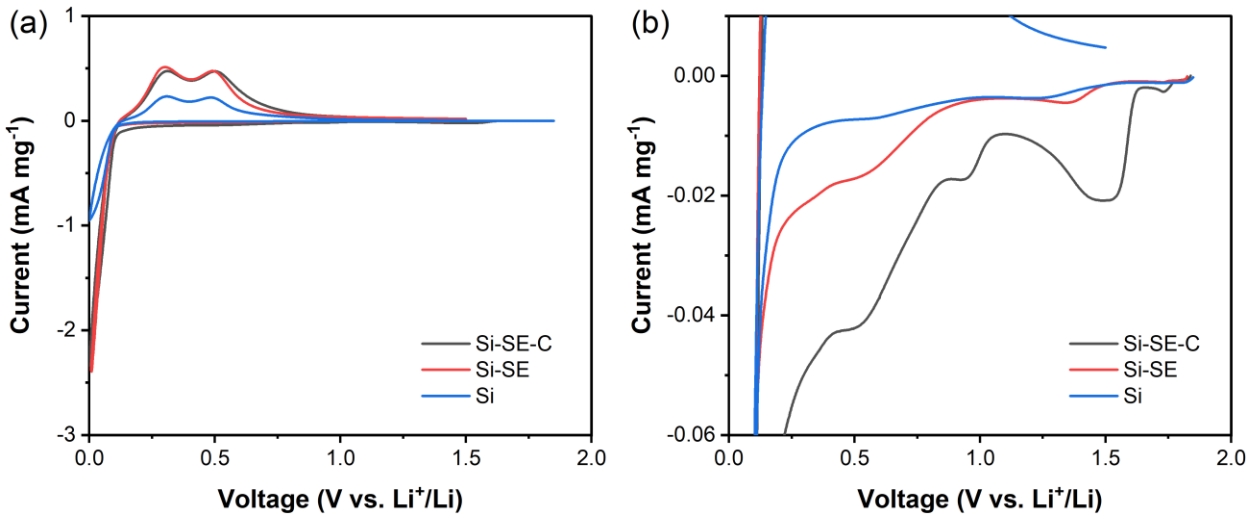

Figure S9 (a) Cyclic voltammetry profiles of Si-SE-C, Si-SE, and Si anodes. (b) The magnified region in (a) to show the details.

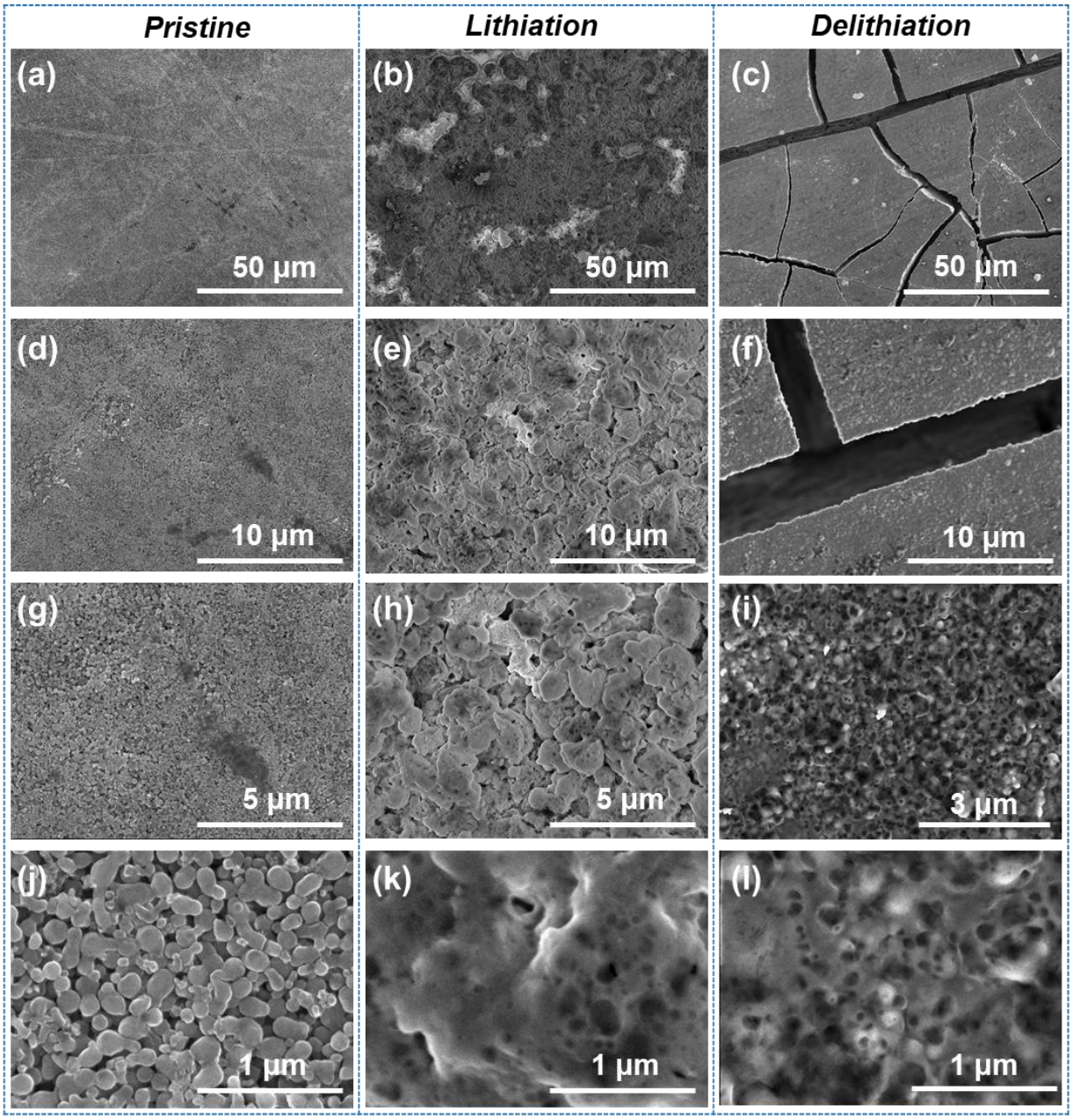

Figure S10. SEM images of Si anode at (a, d, g, j) pristine, (b, e, h, k) lithiation, and (c, f, i, l) delithiation stages at different magnifications.

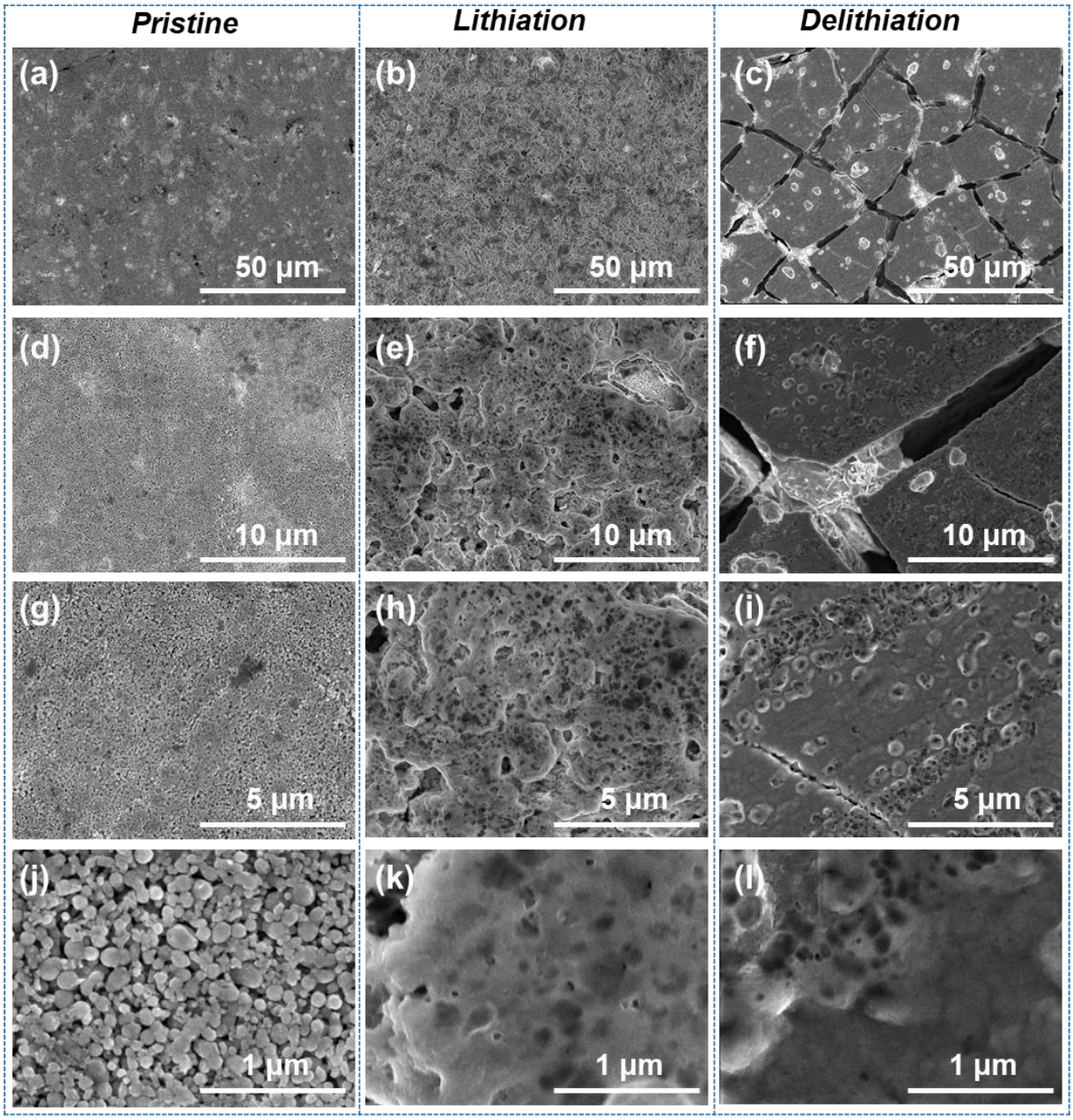

Figure S11. SEM images of Si-SE anode at (a, d, g, j) pristine, (b, e, h, k) lithiation, and (c, f, i, l) delithiation stages at different magnifications.

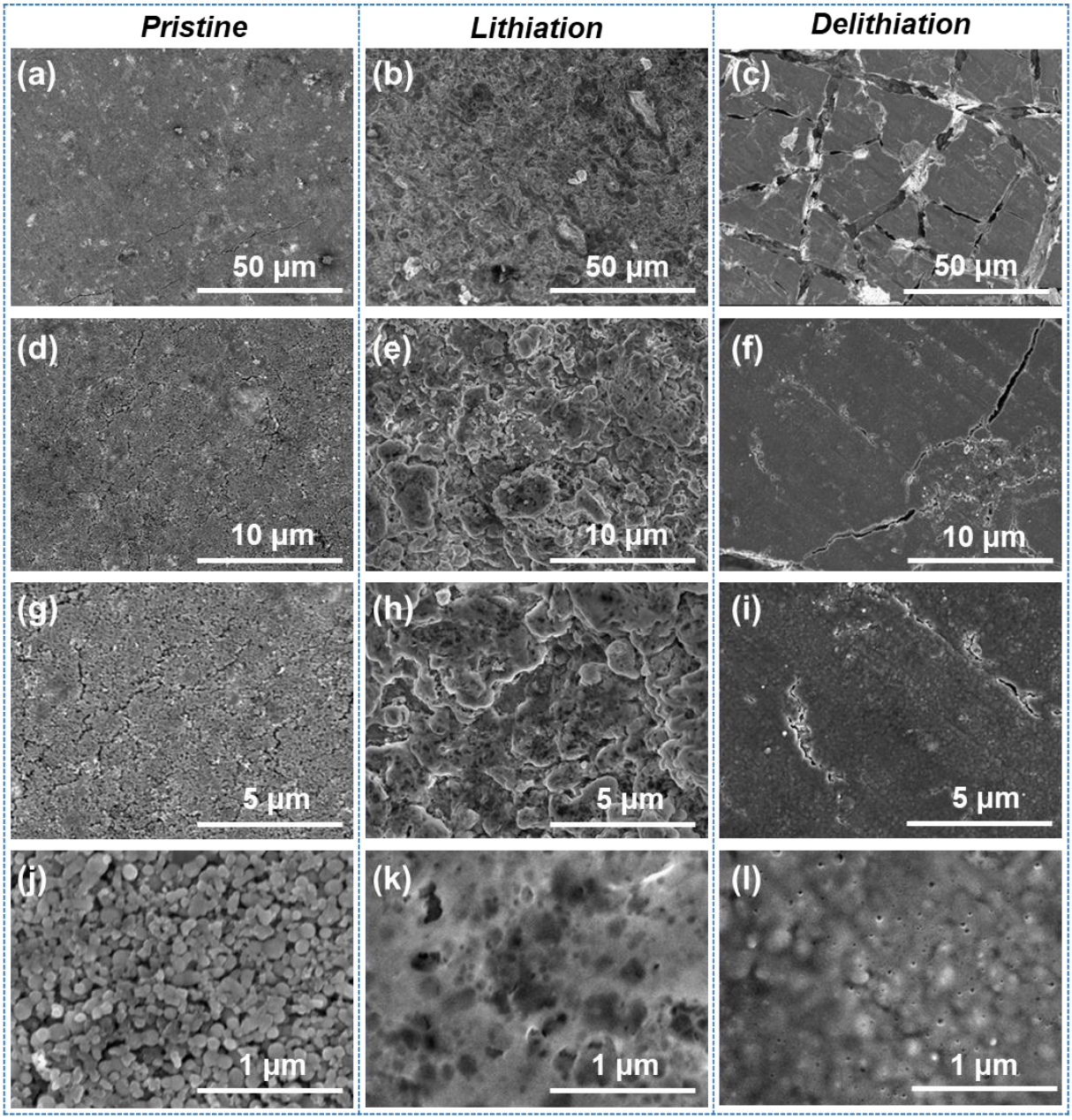

Figure S12. SEM images of Si-SE-C anode at (a, d, g, j) pristine, (b, e, h, k) lithiation, and (c, f, i, l) delithiation stages at different magnifications.

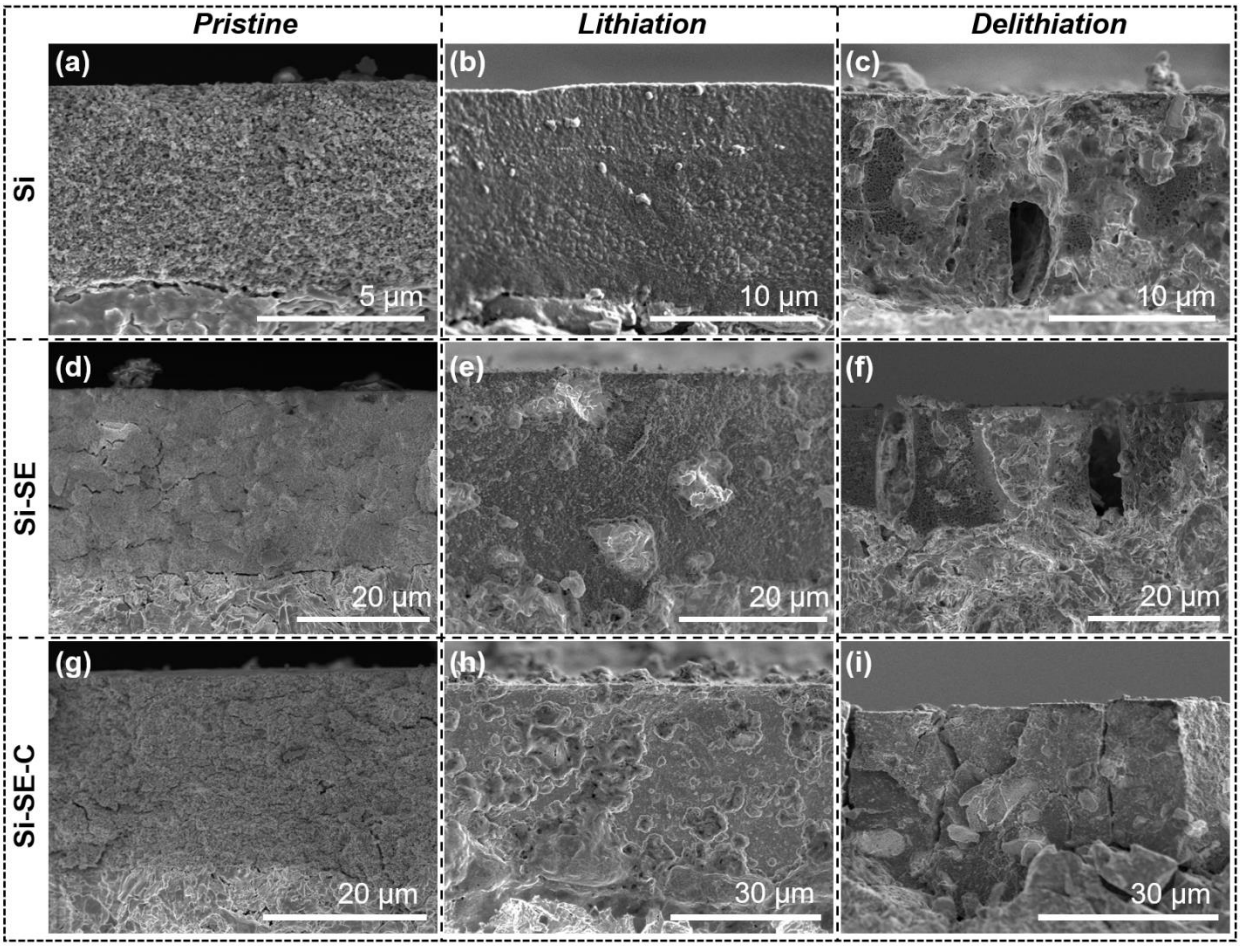

Figure S13. Cross-sectional SEM images of Si at (a) pristine, (b) lithiation, and (c) delithiation states. Cross-sectional SEM images of Si-SE at (d) pristine, (e) lithiation, and (f) delithiation states. Cross-sectional SEM images of Si-SE-C at (g) pristine, (h) lithiation, (i) delithiation states.

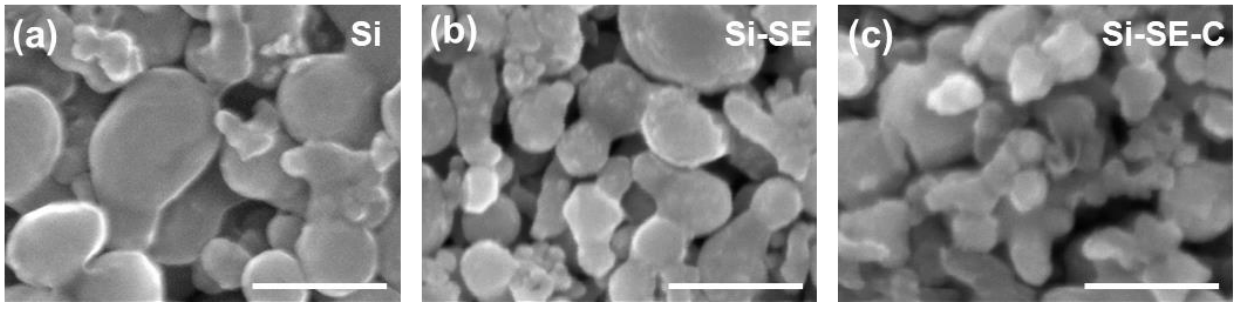

Figure S14. High magnification SEM images of (a) Si, (b) Si-SE, and (c) Si-SE-C anode materials after pressure of 300 Mpa. The scale bar is 200 nm.

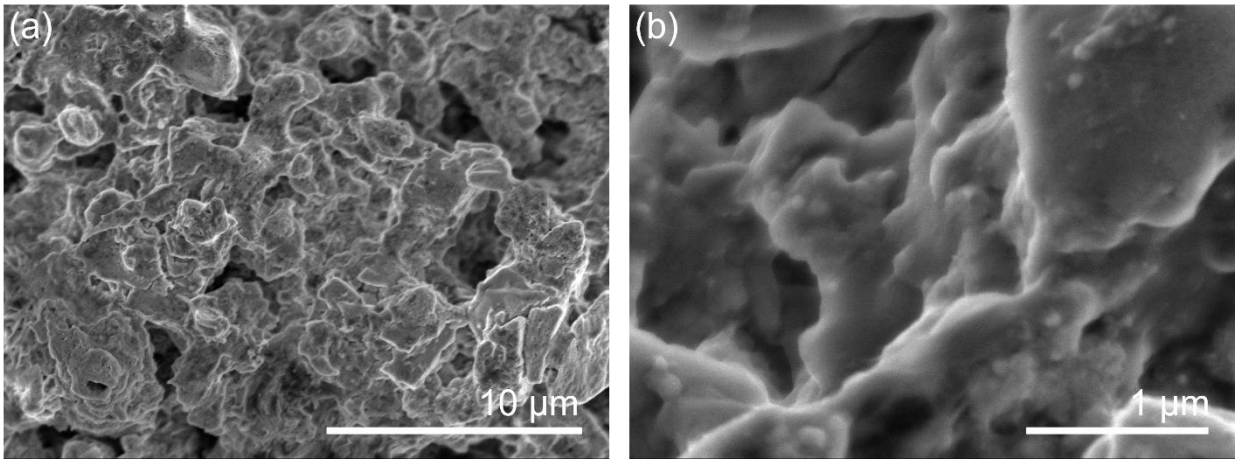

Figure S15. SEM images of SE at (a) 5k× and (b) 35k× magnification.

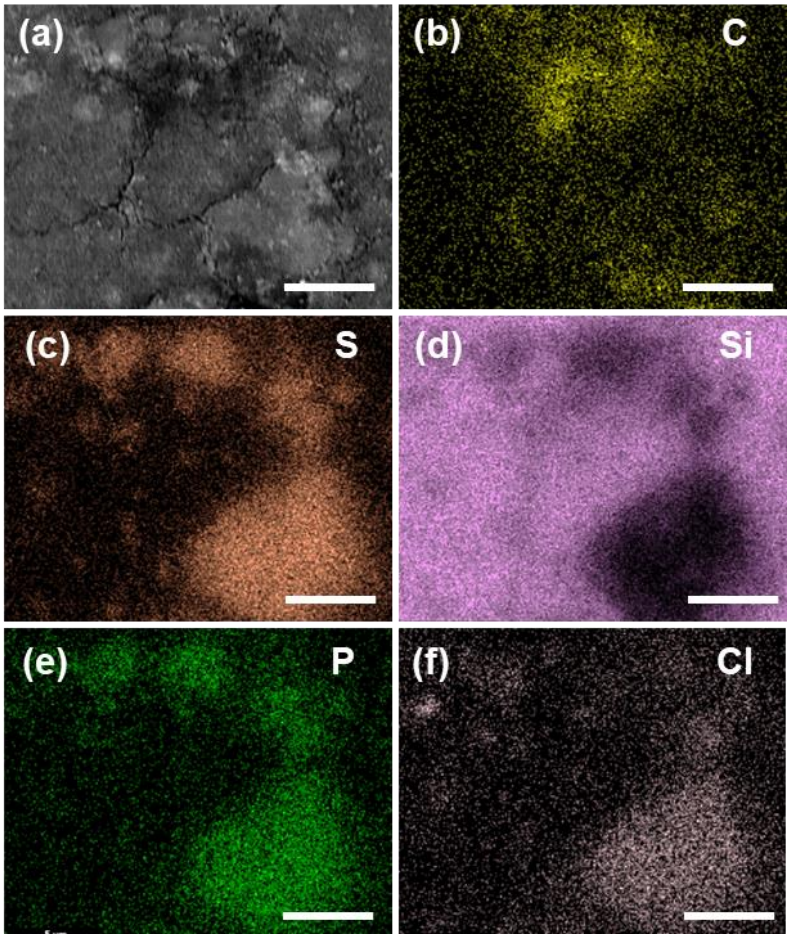

Figure S16. (a) SEM image of Si-SE-C composite anode and (b-f) corresponding EDX element mappings of (b) C, (c) S, (d) Si, (e) P, and (f) Cl. The scale bar is 5 μm.

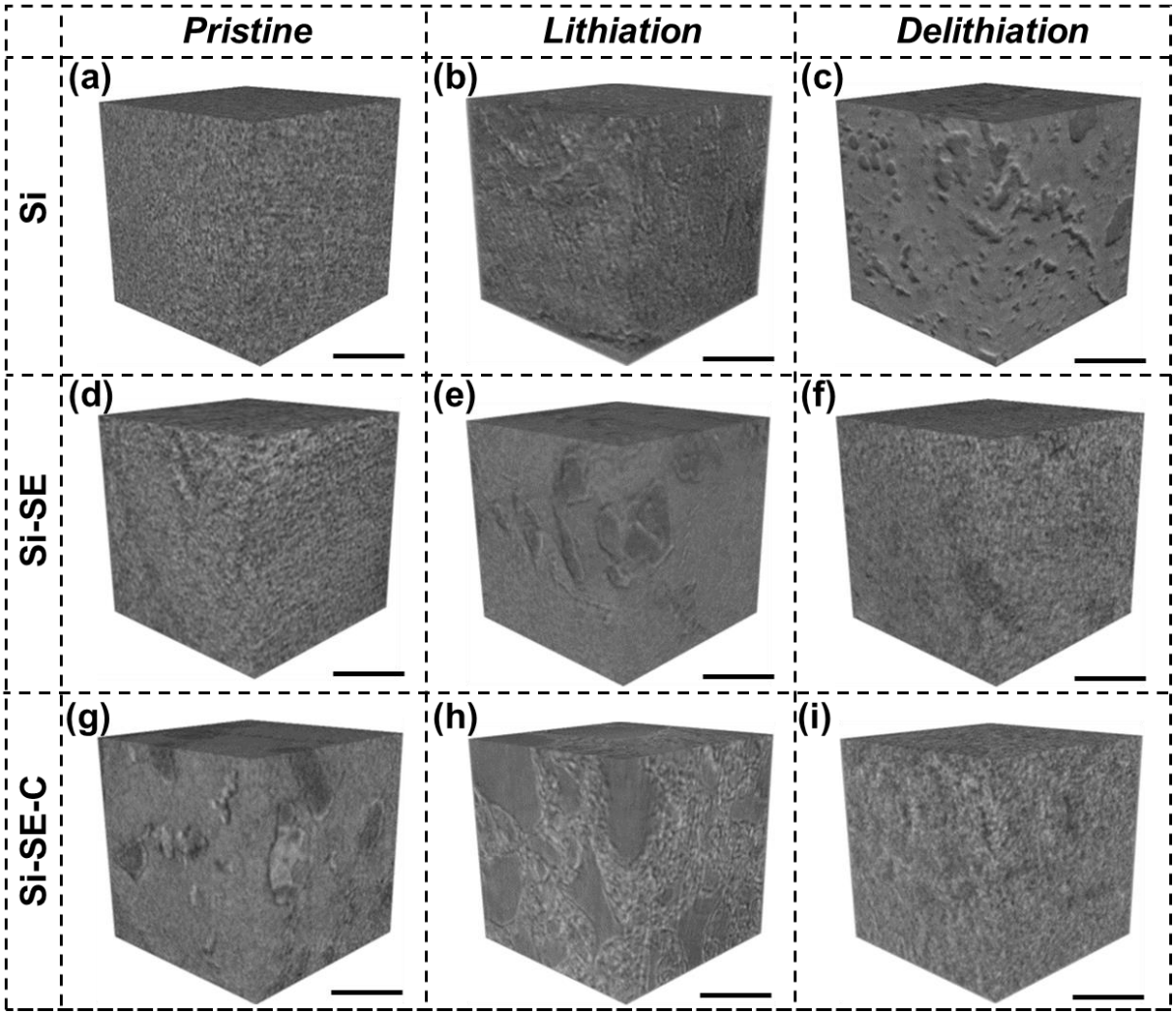

Figure S17. Reconstructed 3D XnT images of Si anode in (a) pristine, (b) lithiation, and (c) delithiation stages. Reconstructed 3D images of Si-SE composite anode in (d) pristine, (e) lithiation, and (f) delithiation stages. Reconstructed 3D images of Si-SE-C composite anode in (g) pristine, (h) lithiation, and (i) delithiation stages. The cube size is 10*10*10 μm^3, and the scale bar is 5 μm.

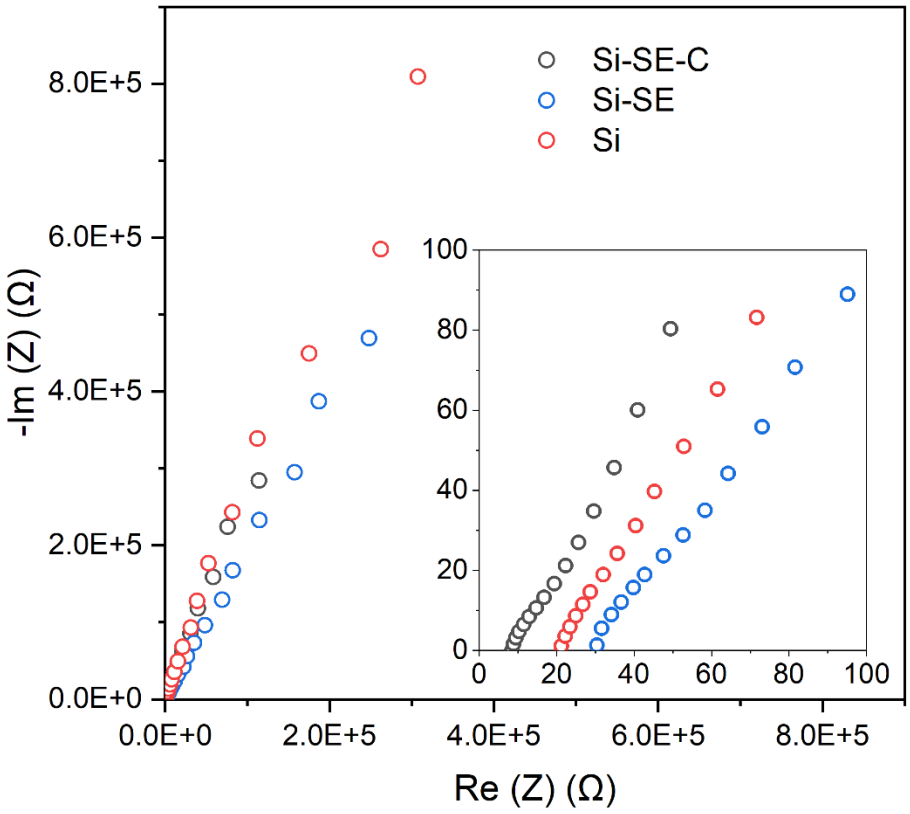

Figure S18. Nyquist plots of three cells before cycling. The inset shows plots at the high-frequency region.

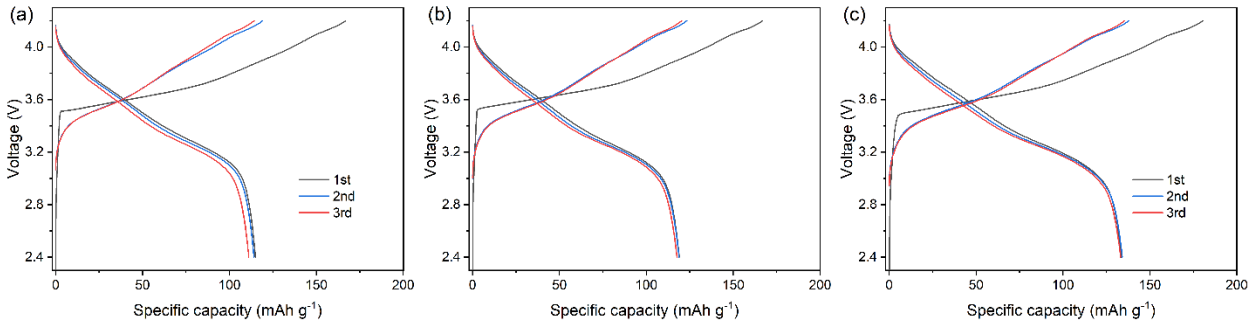

Figure S19. Galvanostatic charge and discharge profiles of full cells using (a) Si, (b) Si-SE, and (c) Si-SE-C anodes in the initial three cycles.

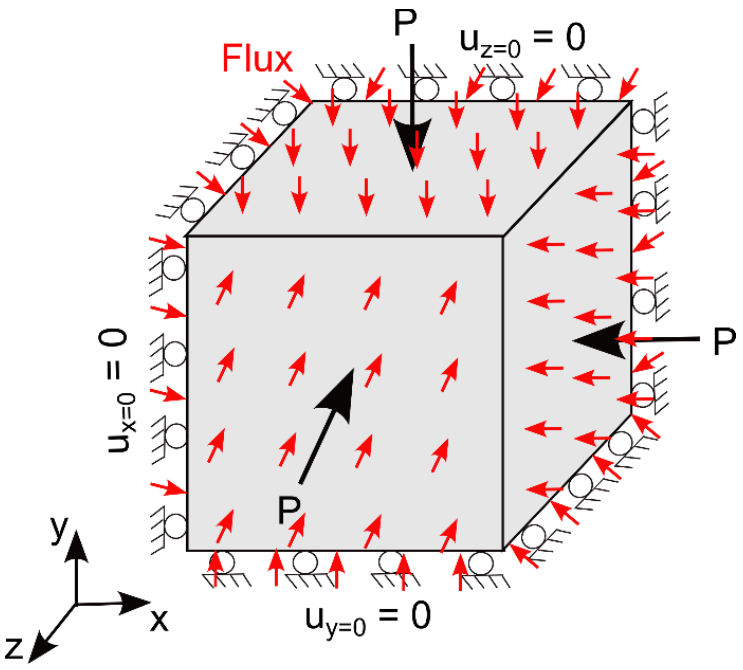

Figure S20. Schematic illustration of boundary conditions to perform the simulation for different anode materials during the lithiation and delithiation process. Left, bottom, and back planes are subjected to roller boundary conditions. Stack pressure (P=150 MPa) is applied on the front, right, and top planes of the cube. The constant flux boundary condition is employed on all six planes of the cube. The cube size is $1.4 \times 1.4 \times 1.4\ \mu m^3$.

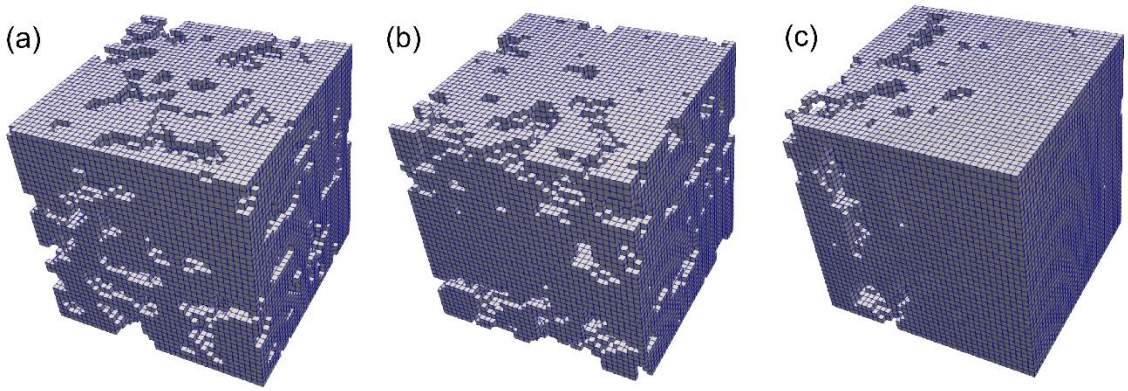

Figure S21. Finite-element mesh for reconstructed microstructure of (a) Si, (b) Si-SE, and (c) Si-SE-C anode materials.

Table S1. Stoichiometry of Li_xSi in Si composite anodes at different SoC and DoD.

Anode	Cycle	SoC					DoD				
		0%	25%	50%	75%	100%	0%	25%	50%	75%	100%
Si-SE-C	1st	Si	$Li_{0.36}Si$	$Li_{0.72}Si$	$Li_{1.08}Si$	$Li_{1.44}Si$	$Li_{1.44}Si$	$Li_{1.21}Si$	$Li_{0.97}Si$	$Li_{0.74}Si$	$Li_{0.50}Si$
	2nd	$Li_{0.50}Si$	$Li_{0.63}Si$	$Li_{0.76}Si$	$Li_{0.88}Si$	$Li_{1.01}Si$	$Li_{1.01}Si$	$Li_{0.88}Si$	$Li_{0.75}Si$	$Li_{0.62}Si$	$Li_{0.49}Si$
Si-SE	1st	Si	$Li_{0.28}Si$	$Li_{0.55}Si$	$Li_{0.83}Si$	$Li_{1.10}Si$	$Li_{1.10}Si$	$Li_{0.99}Si$	$Li_{0.88}Si$	$Li_{0.77}Si$	$Li_{0.66}Si$